

Time Evolution of the Turnover Frequency for Diagnosis of the Coronal Magnetic Field *

Guang-Li Huang

Purple Mountain Observatory, Chinese Academy of Sciences, Nanjing 210008; glhuang@pmo.ac.cn

Received 2005 April 26; accepted 2005 August 30

Abstract Two impulsive microwave bursts observed by Owens-Valley Solar Arrays (OVSA) are studied. The fast time variation of the turnover frequency in these bursts is quite different from the constant value in the earlier conclusion. The observational turnover frequencies are consistent with the calculations using the non-thermal gyro-synchrotron radiation model. We find the turnover frequency may play an important role for calculating the coronal magnetic field on the basis of Dulk and Marsh's approximations.

Key words: Sun: radio radiation — Sun: corona — Sun: magnetic fields

1 INTRODUCTION

The turnover or peak frequency is a useful quantity for diagnosis of solar microwave and hard X-ray spectra (Dulk 1985). However, in solar microwave spectra it does not shift as expected during flare development (Benka et al. 1992), and remains remarkably constant throughout the development of the flare for the majority (Bastian et al. 1998), which may be interpreted by a systematic evolution of the electric field during the course of the flare, or by Razin suppression with a high ambient density of $\geq 10^{11} \text{ cm}^{-3}$.

On the other hand, the time evolution of the turnover frequency has not been much studied so far. Two impulsive events are selected from the observations of the Owens-Valley Solar Arrays (OVSA), and the time evolution of the turnover frequency is compared with the calculation of the non-thermal gyro-synchrotron radiation model in this paper. In Section 2, the two OVSA events are introduced. The time evolution of turnover frequency in the microwave spectra is compared with the theoretical prediction of a non-thermal model of gyro-synchrotron radiations in Section 3. The conclusions are presented in Section 4.

2 OBSERVATION

OVSA is the only dedicated solar radio observatory in the US and therefore plays an important role in supplying the community with high spatial, temporal and spectral resolution microwave data of the solar atmosphere. Currently, the array consists of two 27-m antennas together with four 2-m dishes and observes the Sun at 45 frequencies between 1 and 18 GHz (Hurford et al. 1999). Two events are selected on June 3 and 10, 2000 with impulsive time profiles in both of the microwave bursts (Figs. 1a, 1b).

* Supported by the National Natural Science Foundation of China.

2.1 Example 1

The first event is in AR9026 (N21E61) at 19:10–19:40 UT with maximum at 19:19 UT on 2000 June 3. Its dynamic spectrum is shown in Figure 2, and several spectral profiles before and after the maximum phase are shown in Figure 3. The turnover frequency was evidently changed between 5–15 GHz.

2.2 Example 2

The second event is in the same active region AR9026 (N22W29) at 16:45–17:30 UT with maximum at 16:55 UT on 2000 June 10. Its OVSA dynamic spectrum is shown in Figure 4 and several spectral profiles before and after the maximum phase are shown in Figure 5. The turnover frequency was also changed evidently between 5–10 GHz.

3 TURNOVER FREQUENCY

3.1 Model

The expression of the turnover frequency (or peak frequency) for non-thermal gyro-synchrotron radiation was given in Dulk (1985):

$$\nu_p \approx 2.72 \times 10^3 10^{0.27\delta} \times (\sin \theta)^{0.41+0.03\delta} (NL)^{0.32-0.03\delta} \times B^{0.68+0.03\delta}. \quad (1)$$

Expressions of coronal magnetic field and non-thermal density based on the approximations of Dulk et al. (1982) were derived in earlier papers (Zhou & Karlicky 1994; Huang & Zhou 2000).

$$B = \left[\frac{2.0\Omega_s \nu^2}{S_\nu A_1} \nu_p^{1.3+0.98\delta} \nu^{-0.78-0.9\delta} (2.8 \times 10^6)^{-2.52-0.08\delta} \right]^{\frac{1}{0.52+0.08\delta}}, \quad (2)$$

$$A_1 = 4.24 \times 10^{14+0.3\delta} (\sin \theta)^{0.34+0.07\delta}, \quad (3)$$

$$NL = \left(\frac{S_\nu}{2\Omega_s} \right) A_2^{-1} B^{-1}, \quad (4)$$

$$A_2 = 3.3 \times 10^{-24-0.52\delta} (\sin \theta)^{-0.43+0.65\delta} \left(\frac{\nu}{\nu_B} \right)^{1.22-0.9\delta}, \quad (5)$$

$$N = \int_{E_0}^{\infty} K E^{-\delta} dE = \frac{-K E_0^{1-\delta}}{1-\delta}. \quad (6)$$

Here, B is the magnetic field strength, c the velocity of light in vacuum, k the Boltzmann constant, S_ν the radio flux at a given frequency ν , ν_p the peak frequency or turnover frequency (greater than ν), ν_B the electron gyro-frequency, θ the angle between the wave vector and magnetic field, Ω_s the scale and the solid angle of the source in the bursts, N the total density of the non-thermal electrons above a low cutoff energy E_0 , δ the energetic spectral index of non-thermal electrons with power law distribution ($\delta = (1.22 - \gamma)/0.9$), and γ the radiation spectral index.

It is emphasized that Eqs. (1), (2), and (4) are derived from the emissivity and absorption coefficients under the approximations of Dulk et al. (1982), with the condition of the optical depth $\tau \approx 1$ at ν_p . So, it is possible to calculate B and NL respectively from Eqs. (2) and (4) with observed $\nu_p, \nu, \gamma(\delta)$ and S_ν for assumed values of θ, Ω_s . Substituting Eqs. (2) and (4) into Eq. (1), we obtain a new expression of ν_p :

$$\nu_p = 10^{c_1} (\sin \theta)^{c_2} T_{b\nu}^{c_3} \nu^{c_4}, \quad (7)$$

$$T_{b\nu} = \frac{c^2}{2k\nu^2} \frac{S_\nu}{\Omega_s}, \quad (8)$$

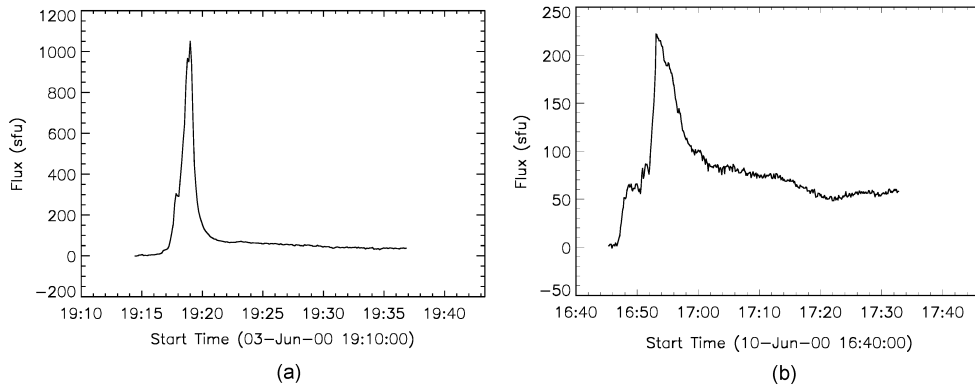


Fig. 1 Time profile of the microwave burst observed by OVSA at a selected frequency (13.2 GHz) on (a) 2000 June 3 and (b) 2000 June 10.

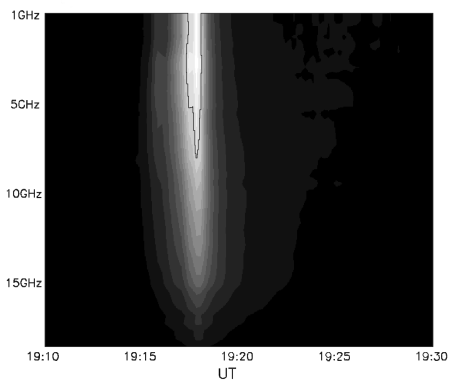


Fig. 2 Dynamic spectrum of the microwave burst observed by OVSA on 2000 June 3.

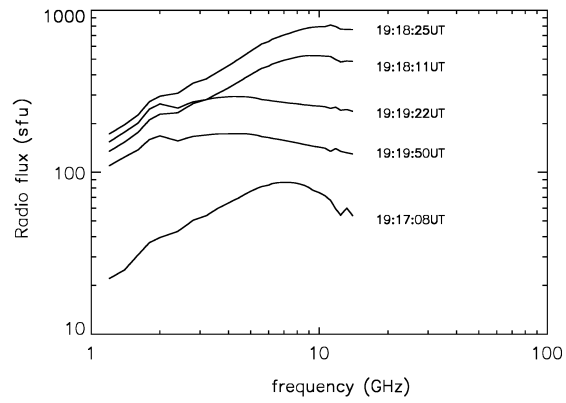


Fig. 3 Spectral profiles of the microwave burst observed by OVSA at selected times on 2000 June 3.

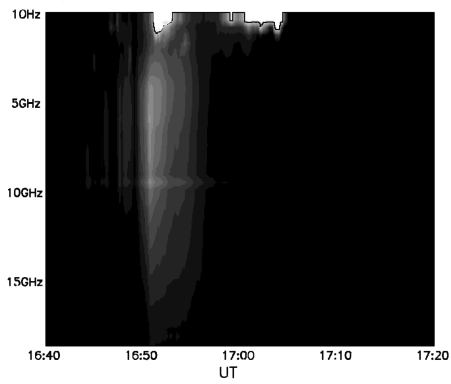


Fig. 4 Dynamic spectrum of the microwave burst observed by OVSA on 2000 June 10.

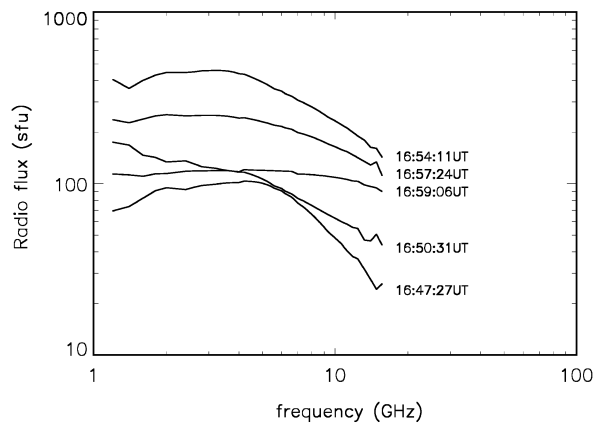


Fig. 5 Spectral profiles of the microwave burst observed by OVSA at selected times on 2000 June 10.

Table 1 Observed Turnover Frequencies ν_{po} and Calculated Turnover Frequencies ν_{pt} at Different Times (t_1 - t_6) on 2000 June 3

	t_1	t_2	t_3	t_4	t_5	t_6
Flux (sfu)	20	160	300	80	50	40
γ	2.0	3.0	2.0	2.3	2.2	2.1
δ	3.6	4.7	3.6	3.9	3.8	3.7
ν (GHz)	1.0	15.0	10.0	4.0	15.0	15.0
ν_{po} (GHz)	0.5	8.0	5.0	2.0	6.0	5.0
ν_{pt} (GHz)	0.52	11.0	3.3	2.8	4.4	3.4
B (G)	0.6	150	43.6	6.6	250	160
$N(10^8 \text{ cm}^{-3})$	21	7.5	1.7	20	0.01	0.1

$$c_1 = \{c_6[(3.4 + 0.27\delta) - c_7(5.5 + 5.3\delta)] + c_5(5.9 - 0.82\delta)\}/c_8, \quad (9)$$

$$c_2 = \{c_6[(0.41 + 0.03\delta) + c_7(0.43 - 0.65\delta)] - c_5(0.34 + 0.07 * \delta)\}/c_8, \quad (10)$$

$$c_3 = (c_6 c_7 - c_5)/c_8, \quad (11)$$

$$c_4 = c_3(0.78 + 0.9\delta)/c_8, \quad (12)$$

$$c_5 = (0.22 - 0.9\delta)(0.32 - 0.03\delta) + (0.68 + 0.03\delta), \quad (13)$$

$$c_6 = 0.52 + 0.08\delta, \quad (14)$$

$$c_7 = 0.32 - 0.03\delta, \quad (15)$$

$$c_8 = c_6 - c_5(1.3 + 0.98\delta). \quad (16)$$

Hence, it is possible to calculate ν_p from Eqs. (7)–(16) with observed ν , $\gamma(\delta)$, S_ν , and assumed θ , Ω_s .

3.2 Discussion

3.2.1 Example 1

Figure 6 gives the time profiles of the radio flux, turnover frequency, and spectral index in the event of 2000 June 3. There is a positive correlation, with a time lag, between the radio flux and the turnover frequency, with an enhancement of the turnover frequency in the decay phase. On the other hand, there is a negative correlation, with some fluctuations between the time evolutions of the turnover frequency and the spectral index. Several times labelled t_1 - t_6 are marked for comparison with the theoretical calculations. First, the magnetic field strength is calculated with Eq. (2), assuming a source size of 10^4 km and an angle of propagation of 60° . Then, the turnover frequency (ν_{pt}) at different times (t_1 - t_6) is calculated with Eq. (7), and compared with the observed values (ν_{po}).

The theoretical turnover frequencies ν_{pt} at t_1 - t_6 are compared with the observed turnover frequencies ν_{po} . The two time evolutions are similar.

3.2.2 Example 2

Figure 7 is the same as Figure 6, but for the event of 2000 June 10. There is again a positive correlation between the radio flux and the turnover frequency with a time lag, and a negative correlation between the turnover frequency and spectral index with some fluctuations. However, there is no enhancement of the turnover frequency after the impulsive phase as in Figure 6. Six time instants labelled t_1 - t_6 are selected, and the turnover frequency at these instants is calculated and compared with the observed values.

The results in Table 2 are quite similar to those in Table 1, i.e., the calculated turnover frequencies at t_1 - t_6 are comparable to the observed ones in both tendency and magnitude.

In Figure 8, we plot the observed ν_{po} against the calculated ν_{pt} , with different symbols for the two events. We note that the data points are distributed close to the diagonal line, $\nu_{po} = \nu_{pt}$.

Moreover, Figures 9a and 9b indicate that the fast time variations of ν_p in these two events are well explained by the theory of gyro-synchrotron emissions under Dulk & Marsh's approximations.

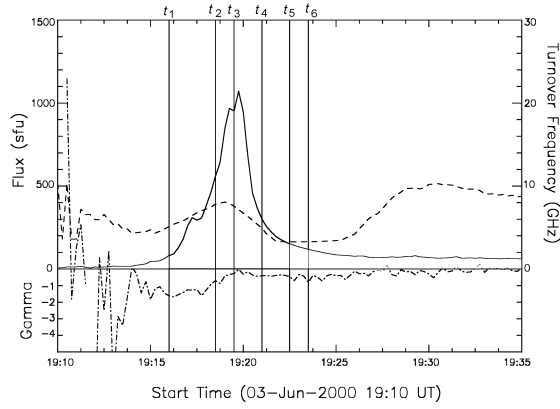


Fig. 6 Time profiles of the flux (solid line), the turnover frequency (dashed line) and the spectral index (dot-dashed line) of the microwave burst of 2000 June 3. OVSA observations.

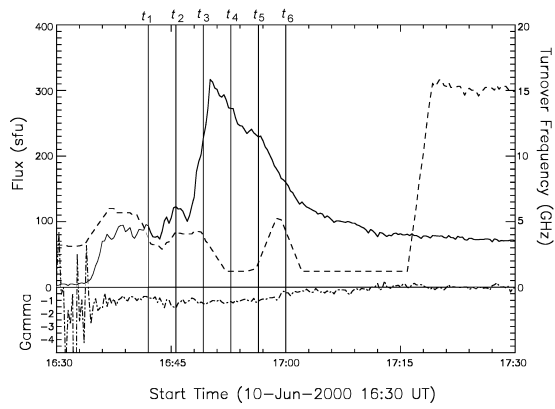


Fig. 7 Time profiles of the flux (solid line), the turnover frequency (dashed line) and the spectral index (dot-dashed line) of the event of 2000 June 10. OVSA observations.

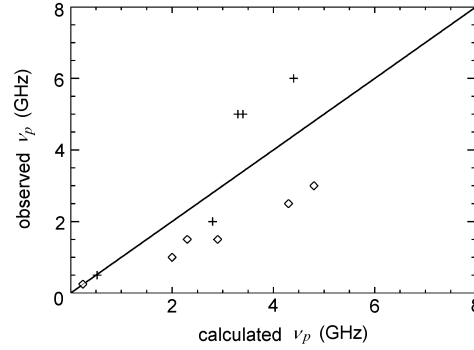


Fig. 8 A comparison between ν_{po} and ν_{pt} for the June 2 event (cross) and the June 10 event (triangles). The diagonal line $\nu_{po} = \nu_{pt}$ is shown.

Table 2 Turnover Frequencies in Observations (ν_{po}) and Calculations (ν_{pt}) at Different Times ($t_1 - t_6$) on 2000 June 10

	t_1	t_2	t_3	t_4	t_5	t_6
Flux (sfu)	15	60	60	150	180	120
γ	2.0	2.8	2.4	2.7	2.3	2.4
δ	3.6	4.5	4.0	4.3	3.9	4.0
ν (GHz)	0.4	5.0	2.5	5.0	2.0	3.0
ν_{po} (GHz)	0.25	2.5	1.5	3.5	1.0	1.5
ν_{pt} (GHz)	0.24	4.3	2.3	4.8	2.0	2.9
B (G)	0.7	14.1	17.4	23.0	11.0	0.7
$N(10^9 \text{ cm}^{-3})$	0.2	1.1	1.3	3.6	1.6	3.0

3.3 Turnover Frequency and Frequency Drift

The turnover frequency is associated with the frequency drift: if the peak time is different at different frequencies, then obviously the peak frequency will be different at different times.

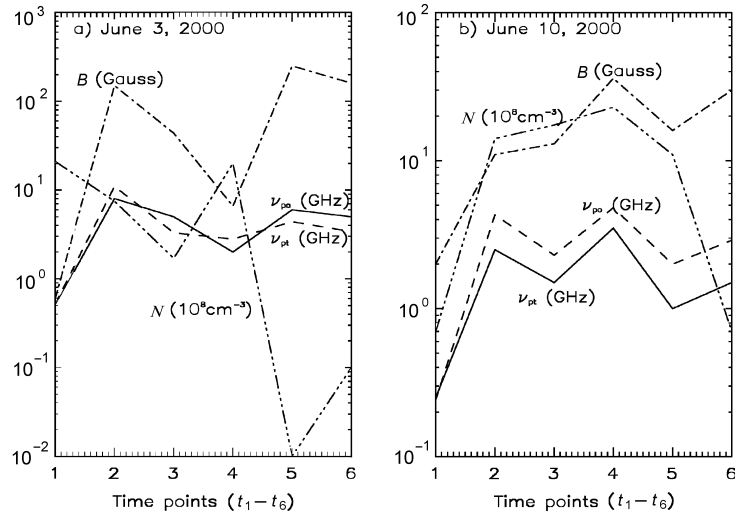


Fig. 9 Time profiles of ν_{po} (solid line) and ν_{pt} (dashed line), B (dot-dashed line), and N (dot-dot-dot-dashed line) in (a) the June 3 event and (b) the June 10 event.

It is found that the peak times are almost fixed at different frequencies in these two events, hence, there is no frequency drift in these two events (Figs. 2 and 4). However, it does not imply that the turnover frequency does not shift in the two events, because variation of the turnover frequency not only depends on the delay of the peak time, but also on the shape of the time profile at different frequencies. The turnover frequency is the maximum frequency at different times in a given event, and the fast variation of the turnover frequency is found to correspond to the impulsive time profiles shown in Figures 3 and 5.

On the other hand, when it is difficult to calculate a very fast frequency drift due to the limitations of time resolution, it may not be so difficult to calculate the turnover frequency, i.e., the maximum frequency, at different times, though the mechanism of frequency drift (caused by a moving source) is quite different from that of the turnover frequency.

3.4 Effect of Turnover Frequency on the Calculation of Magnetic Field and Non-thermal Electron Density

The magnetic field and the density of non-thermal electrons are calculated for t_1 - t_6 of the two events and listed in Tables 1 and 2 and shown in Figures 9a and 9b. The calculated magnetic field is directly proportional to the turnover frequency and the spectral index, and inversely proportional to the radio flux (see Figs. 6-7 and Eq. (2)). However, the time variation of the non-thermal electron density in Figures 9a and 9b is not evidently associated with that of the turnover frequency.

4 CONCLUSIONS

The time evolution of the turnover frequency in solar microwave bursts is studied with data of OVSA, and is found to be basically consistent with the prediction of the non-thermal gyro-synchrotron radiation model. The fast time variation of the turnover frequency is quite different from the conclusion in the earlier paper that the turnover frequency is remarkably constant.

Moreover, the turnover frequency may play an important role in a self-consistent calculation of the coronal magnetic field and non-thermal electrons from the measured brightness temperature, frequency, turnover frequency, and spectral index in a given solar microwave burst.

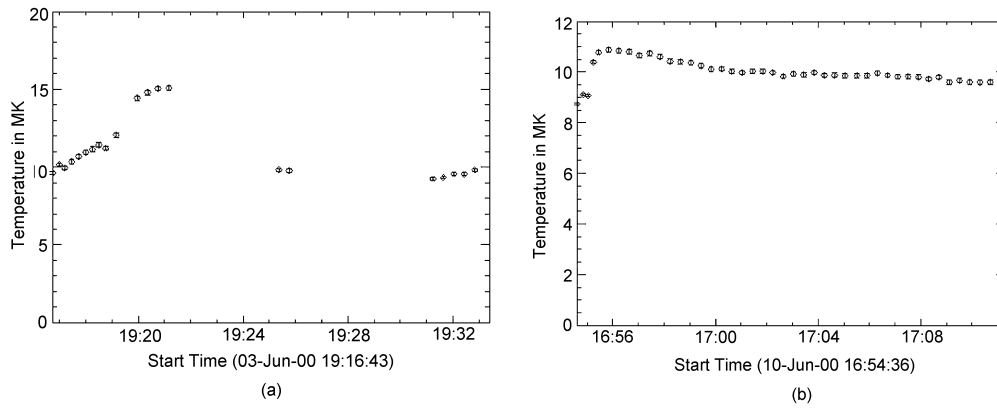


Fig. 10 Time evolutions of the plasma temperature calculated from YOHKOH/SXT (a) on 2000 June 3, and (b) on 2000 June 10.

It is emphasized that the approximations of Dulk et al. (1982) can only be used under the conditions of $2 < \delta < 7$, $10 < S < 100$ (S is the harmonic number), $E_0 = 10$ keV, and $\theta \sim 20^\circ - 80^\circ$, here ν_p is defined as the frequency at optical depth $\tau \approx 1$, and for the X-mode emission. Also, these approximations can be used only for a simple and isolated source without significant variations in the magnetic field, the angle etc., along the line-of-sight within the emission region. If these conditions are not satisfied, then there could be very large errors in the estimations of magnetic field and non-thermal electrons from Eqs. (2)–(6).

On the other hand, the pure non-thermal gyro-synchrotron models can only be used around the peak time of the impulsive bursts, such as t_2 – t_3 in Table 1 and t_4 – t_5 in Table 2, in which the harmonic numbers are still in the range between 10–100. A very larger harmonic number at several time points in Tables 1 and 2 just mean that the thermal gyro-synchrotron emissions should be taken into consideration. The local plasma temperatures in these two events are up to 10 MK as shown in Figure 10.

Moreover, the lower cutoff energy E_0 is a key parameter when determining the total density of the non-thermal electrons above the cutoff. It is shown in a recent paper by the present author that the low cutoff energy is very sensitive to the calculations of the magnetic field in the model of non-thermal gyro-synchrotron radiation (Huang et al. 2005). However, the value of E_0 is fixed as 10 keV in the approximations of Dulk et al. (1982). Hence, the calculation of coronal magnetic field is not self-consistent under the approximations of Dulk et al. (1982).

Acknowledgements This study is supported by the NFSC Grants 10333030 and 10273025, and “973” program G2000078403. The author should thank Dr. D. E. Gary for helpful discussions and usage of the OVSA data.

References

- Bastian T. S., Benz A. O., Gary D. E., 1998, *ARA&A*, 36, 131
- Benka S. G., Holman G. D., 1992, *ApJ*, 391, 854
- Dulk G. A., Marsh K. A., 1982, *ApJ*, 259, 350
- Dulk G. A., 1985, *ARA&A*, 23, 169
- Huang G. L., Zhou A. H., 2000, *New Astron.*, 4, 591
- Huang G. L., Zhou A. H., Su Y. N. et al., 2005, *New Astron.*, 10, 219
- Hurford G. J., Gary D. E., Bastian T. S. et al., 1999, *Bulletin of the American Astron. Soc.*, 31, 956
- Zhou A. H., Karlicky M., 1994, *Solar Phys.*, 153, 441